Real-Time Beam Visualization for Monitoring External Beam Radiotherapy: A Feasibility Study

Cesare Jenkins[1,2], Dominik Naczynski[1], Shu-Jung Yu[1], and Lei Xing[1]

[1] Department of Radiation Oncology, Stanford University School of Medicine, Stanford, CA, USA,
[2] Department of Mechanical Engineering, Stanford University, Stanford, CA, USA

Abstract. As external beam radiation therapy has advanced in complexity and precision there have been few new tools developed to monitor the accuracy of treatment delivery. To this end, a system for real-time beam visualization (RT-BV) was developed. The system consists of a flexible scintillating film, common optical detectors and image processing algorithms. The scintillating films were formed by mixing Gd_2O_2S:Tb (GOS) with silicone. The films were placed in the path of therapeutic beams generated by a medical linear accelerator (LINAC). The emitted light was captured by cameras and processed. The RT-BV system was able to achieve sufficient contrast-to-noise at 20 frames/second with normal ambient room lighting. Pixel intensities were found to be linear with dose-rate and the system demonstrated sub-millimeter resolution in identifying collimator movements.

Keywords: Image Guided Radiation Therapy · Quality Assurance · Cameras

1 Introduction

Each year, thousands of radiation therapy (RT) treatments are performed accurately. However, reports indicate that between 0.6 to 4.7 incidents per 100 radiation therapy visits have been reported to occur even in advanced oncology centers operating with modern equipment and trained staff [1,2,3,4]. A significant number of these incidents occur during the delivery of RT and can result in underdosing or overdosing patients, irradiating healthy tissue or, at worst, patient death [5]. As EBRT techniques continue to increase in complexity and dose delivered per fraction, there is a clear and growing need for a monitoring and validation methodology that enables clinicians to have greater confidence that they are delivering the planned dose where and how it was intended [6].

In current practice, on-board MV electronic portal imaging (EPID) is utilized for monitoring the RT beam after it exits the patient [7]. However, due to a lack of soft tissue contrast and multileaf collimator (MLC) blockage of the field of view, the available anatomic references provided by the approach are limited

to bony anatomy or implanted fiducial markers that lie within the beam's eye view making the interpretation of the data non-trivial [8,9]. More recently Jarvis et al. have presented work demonstrating the potential of Cherenkov emission as a means of visualizing therapy in real time [10]. Fahimian et al. also proposed a method of utilizing air scintillation to visualize the radiation beam [11]. While both seek to visualize therapeutic beam delivery, the signals generated are at least three orders of magnitude smaller than typical room lights [12]. The technical complexity involved in utilizing such techniques has limited their implementation. Hence, the ability to visualize the position, shape and intensity of the radiation beam as it passes through the patient in real-time is not yet available in clinical practice.

As a first step toward developing a system capable of realizing this ability, we developed a simple imaging approach utilizing a flexible scintillating film and an inexpensive digital camera to image the radiation beam as it enters or exits the patient's anatomy.

2 Materials and Methods

The real-time beam visualization (RT-BV) system consists of a flexible scintillating film and a digital camera. The film is placed on the patient's skin such that it will emit an optical signal when the beam passes through it. The camera is arranged such that it can image the emitted signal as well as the surrounding patient surface anatomy.

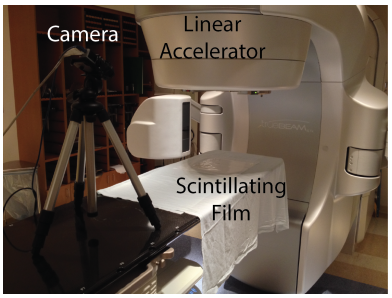

Fig. 1. Photograph of the imaging setup.

The desirable features of a scintillation film to be placed on the patient include ample signal generation, minimal dose attenuation and sufficient flexibility to conform to anatomy. In our study, scintillating films were prepared by mixing GOS powder and a silicone elastomer in a 1:1 mass ratio. The resulting mixture was cast on a level surface at a thickness of 0.8 mm and allowed to cure at room temperature.

The imaging setup, shown in Figure 1, consisted of a 2048 x 2048 CMOS digital camera equipped with a 50 mm lens and a band-pass filter. The camera

was placed 100 cm inferior and 50 cm anterior of iso-center. The halogen lights in the treatment room were set to maximum intensity for all image acquisition. The camera was selected primarily based on its resolution, bandwidth, and cost with secondary consideration given to noise characteristics. All images were acquired with a 42 ms integration time with the gain of the camera set to its minimum value. At this integration time a frame rate of 23 frames per second (fps) is achievable. In general, a set of data for a static field was created by sampling 10 frames over a 2 second interval. Images were analyzed using ImageJ 1.47v (National Institute of Health, Bethesda, MD), Matlab 7.8.0 (The MathWorks Inc. Natick, MA) and OpenCV.

Radiation was delivered using Varian EX and TrueBeam medical linear accelerators (LINAC) (Varian Medical Systems, Palo Alto, CA). Beam energies between 6 and 15 MV were investigated with dose rates ranging between 200 and 600 MU/min. Square fields were delivered while imaging. Bright outliers, caused by x-ray interactions with the imaging sensor were median filtered and a background image was subtracted from each frame. Average pixel values and contrast-to-noise ratios (CNR) where evaluated. See Figure 2 for a graphical overview of the image processing approach.

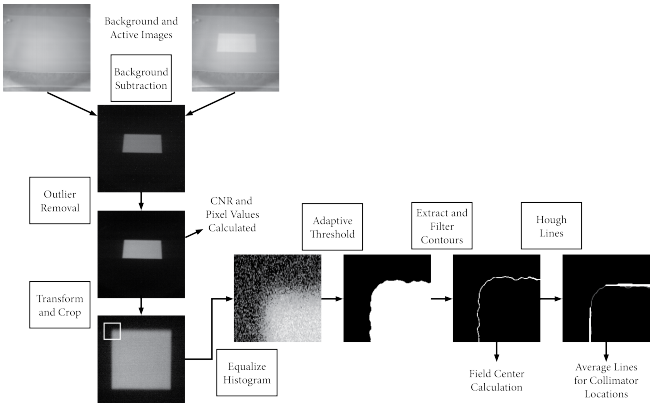

Fig. 2. An overview of the image processing algorithm used to evaluate images and locate field edges. The left column indicates processing that was applied to all images. The small square region indicates the image area magnified at right for demonstrating the localization portion of the algorithm.

In order to verify the resolution and beam shape fidelity of the system, complex MLC shaped fields with gaps ranging from 0.1 cm to 8 cm were delivered and imaged simultaneously with the RT-BV system and a Varian EPID portal imaging system (see Figure 4a). Finally, a full VMAT plan was imaged as it was delivered to an anthropomorphic phantom.

An image processing algorithm was designed to robustly identify and locate the beam within each image in a beam-on dataset. Refer to Figure 2 for a graphical overview of the image-processing algorithm utilized.

A perspective transformation was determined from extracting the corners of a square field in a test image and used to correct for the distortion introduced due to the angled positioning of the camera. The Otsu method was used to identify a threshold value that would best segment the resulting images [13]. A binarization based on this value was applied to the images. Connected components were extracted from the binary images using the algorithm presented by Suzuki et al. [14]. The contours were then filtered by size to identify one that corresponds to the beam profile. The center of the field was calculated from the mass center of the pixels along the identified contour. The outline of the contour was then fit for straight lines using a probabilistic Hough Transform [15]. Lines were grouped according to their angle and location within the image to identify each of the four collimators. An average location for each group was calculated from

$$c_d = \frac{\sum \bar{d} l e^{-|\delta|}}{\sum l e^{-|\delta|}} \tag{1}$$

where c_d is the reported collimator location, $\bar{d}$ is the average pixel coordinate for each line (in the direction of interest), l is the length of the line and δ is the angular deviation of the line from the ideal collimator direction (i.e. 90° for the x-collimators).

3 Results and Discussion

The fabricated films were confirmed to have a thickness of 0.8 mm ± 0.1 mm. They were flexible and molded easily to the contours of an anthropomorphic phantom (Figure 5).

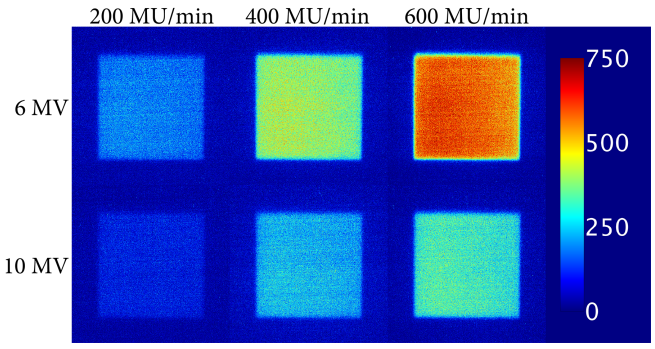

Fig. 3. Images of 10 cm x 10 cm fields at various beam settings. Pixel intensities are reported in arbitrary units.

Processed images of 10 x 10 cm fields for 6 and 10 MV beams with dose rates between 200 and 600 MU/min are shown in Figure 3. Images show clear field boundaries and reasonable uniformity across the field. For beams delivered at a higher dose rate, the penumbra of the beam can also be observed. Pixel intensity values increased with dose rate in a highly linear (R2¿0.97) fashion (data not shown). Increasing beam energy reduces the slope of this relationship. This is consistent with the reduction, at higher energies, in the rate at which dose is deposited at the surface. The average contrast-to-noise (CNR) for sets of 10 images at each beam setting is reported in Table 1. The standard deviation is also presented offering insight into the variation in measurements. These results indicate that the system is capable of monitoring beams across the clinical range in the presence of full room lighting.

Table 1. CNR (SD) for 10 x 10 cm fields at various beam settings.

	Dose rate (MU/min)		
Beam energy (MV)	300	400	600
6	4.0 (0.11)	9.4 (0.38)	18.7 (0.82)
10	1.9 (0.12)	4.9 (0.16)	8.6 (0.32)

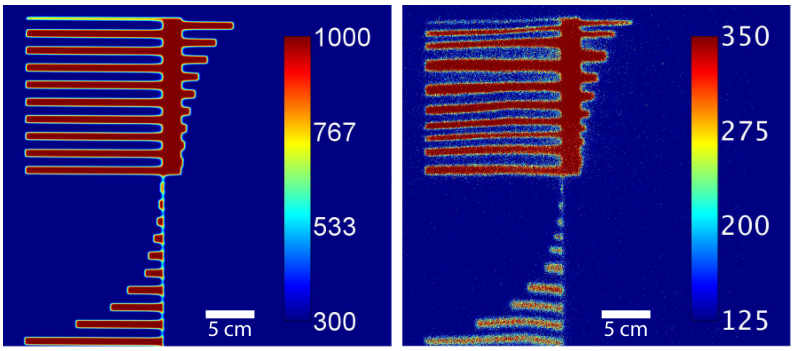

Fig. 4. Images of a test field imaged simultaneously with an EPID portal imaging system (a) and the RT-BV system (b).

Figure 4 shows the result of a simultaneous acquisition with an EPID portal imager and the presented system for a complex test field. All features are discernible, including those created by 1 mm leaf movements near the center of the field. A discernible difference is also observable between features created by leaf

locations that vary by 1 mm. The distortions in the RT-BV system image are due to the fact that the film was not perfectly flat on the couch at the time of imaging. While these distortions are undesirable on a flat surface, they demonstrate the ability of the film to represent the field shape as it appears on the contours of a patients anatomy. Several frames from the imaged VMAT plan are presented in Figure 5. The field, film and phantom are all visible. This test also confirmed that the system was also capable of imaging beam exit profile as well as entry. The algorithm was generally able to properly locate the collimators well within the 1 mm machine tolerance (see Figure 6). The average deviation between machine and estimated locations was 0.5 mm. The maximum deviation was 2mm.

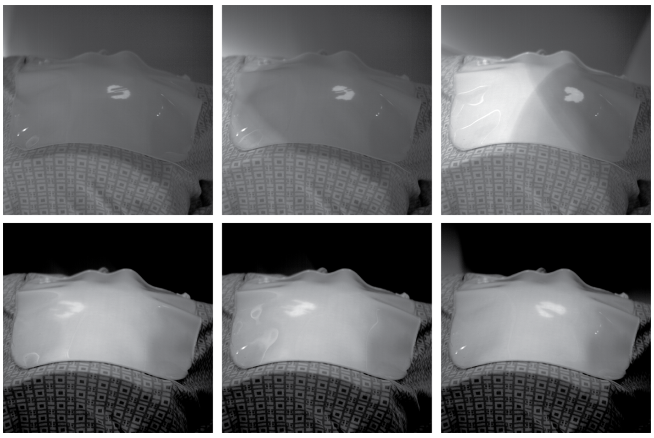

Fig. 5. Sequential images of a VMAT plan being delivered to an anthropomorphic phantom. The top three frames show an entry beam profile as the gantry moves from approximately 0° to 30°. The bottom three frames show a beam exit profile as the gantry moves from approximately 70° to 90°. Full video is available at `http://youtu.be/X6n-aDPBDGw`.

Imaging approaches based on air scintillation [11] or Cherenkov radiation [10] also offer the ability to visualize the beam. These techniques enjoy the advantage of not perturbing the treatment beam but generally require much more advanced imaging setups and image processing. The data presented here was collected using cameras costing approximately $1,500 as compared with an minimum cost of $10,000 for the cameras needed to perform air scintillation or Cherenkov imaging. EPID based techniques measure the beam aperture exiting the patient, but interpreting the data relative to patient anatomy is non-trivial. The proposed system enables high-resolution images of the beam in a context that is immediately interpretable. It also offers the potential for gathering beam dosimetry data at beam entry based on the intensity of emitted optical signal from the film. A combined use of EPID and the RT-BV system may be valuable

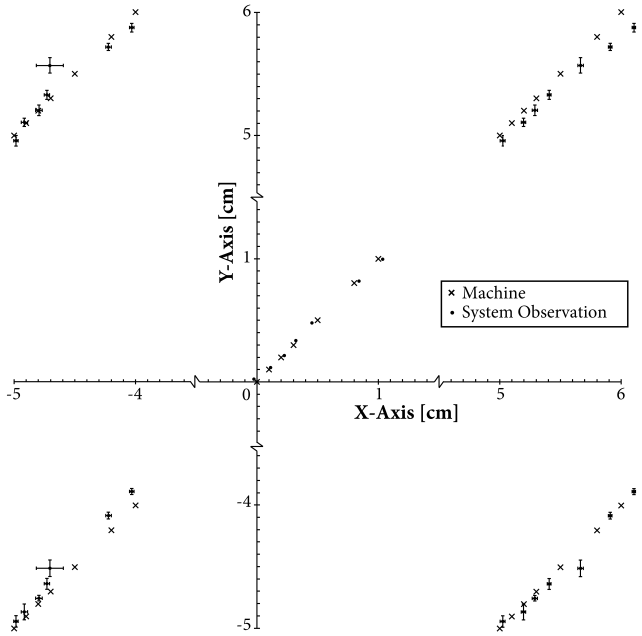

Fig. 6. The results of the collimator location algorithm.

and allow us to harness the strengths of both systems to provide a complete view of therapy.

In summary, the RT-BV system has demonstrated the capability of obtaining high CNR images of therapeutic beams and treatment context in real time. Processing of these images resulted in accurate, sub-millimeter identification of collimator locations. It is envisioned that the proposed system could be used to provide a real-time view/recording of the patient treatment delivery process. While further developments leading to a quantitative, automated system for assessing treatment validity would be ideal and are currently being explored, the availability of qualitative information on beam intensity, shape and location in the context of the patient's anatomical contours offers a valuable, high level view of treatment.

References

1. Morganti, A.G., Deodato, F., Zizzari, S., Cilla, S., Digesu', C., Macchia G., Panuni, S., Gaetano, A.D., Piermattei, A., Cellini, N., Valentini, V.: Complexity index (COMIX) and not type of treatment predicts undetected errors in radiotherapy planning and delivery. Radiother. Oncol. 89, 320-329 (2008)
2. Yeung, T.K., Bortolotto, K., Cosby, S., Hoar, M., Lederer, E.: Quality assurance in radiotherapy: evaluation of errors and incidents recorded over a 10 year period. Radiother. Oncol. 74, 283-291 (2005)

3. Huang, G., Medlam, G., Lee, J., Billingsley, S., Bissonnette, J.P., Ringash, J., Kane, G., Hodgson, D.C.: Error in the delivery of radiation therapy: results of a quality assurance review. Int. J. Radiat. Oncol. Biol. Phys. 61, 1590-1595 (2005)
4. Bissonnette, J.P., Medlam, G.: Trend analysis of radiation therapy incidents over seven years. Radiother. Oncol. 96, 139-144 (2010)
5. Shafiq, J., Barton, M., Noble, D., Lemer, C., Donaldson, L.J.: An international review of patient safety measures in radiotherapy practice. Radiother. Oncol. 92, 15-21 (2009)
6. Yorke, E., Gelblum, D., Ford, E.: Patient safety in external beam radiation therapy. AJR Am. J. Roentgenol. 196, 768-772 (2011)
7. Wiersma, R.D., Mao, W., Xing, L.: Combined kV and MV imaging for real-time tracking of implanted fiducial markers. Med. Phys. 35, 1191-1198 (2008)
8. Timmerman, R.D., Xing, L.: Image-guided and Adaptive Radiation Therapy. Lippincott Williams & Wilkins (2009)
9. Berbeco, R.I., Hacker, F., Ionascu, D., Mamon, H.J.: Clinical Feasibility of Using an EPID in cine Mode for Image-Guided Verification of Stereotactic Body Radiotherapy. Int. J. Radiat. Oncol. Biol. Phys. 69, 258-266 (2007)
10. Jarvis, L.A., Zhang, R., Gladstone, D.J., Jiang, S., Hitchcock, W., Friedman, O.D., Glaser, A.K., Jermyn, M., Pogue, B.W.: Cherenkov video imaging allows for the first visualization of radiation therapy in real time. Int. J. Radiat. Oncol. Biol. Phys. 89, 615-622 (2014)
11. Fahimian, B., Ceballos, A., Trkcan, S., Kapp, D.S., Pratx, G.: Seeing the invisible: Direct visualization of therapeutic radiation beams using air scintillation. Med. Phys. 41, 010702 (2014)
12. Glaser, A.K., Zhang, R., Davis, S.C., Gladstone, D.J., Pogue, B.W.: Time-gated Cherenkov emission spectroscopy from linear accelerator irradiation of tissue phantoms. Opt. Lett. 37, 1193-1195 (2012)
13. Otsu, N.: A threshold selection method from gray-level histograms. IEEE Trans. Syst. Man Cybern. 9, 62-66 (1979)
14. Suzuki, S., be K.: Topological structural analysis of digitized binary images by border following. Computer Vision, Graphics, and Image Processing 30, 32-46 (1985)
15. Matas, J., Galambos, C., Kittler, J.: Robust Detection of Lines Using the Progressive Probabilistic Hough Transform. Comput. Vis. Image Und. 78, 119-137 (2000)